JOURNAL OF MATERIALS SCIENCE 28 (1993) 3235–3242

Microstructures and calorimetric evaluation of non-equilibrium states in rapidly solidified Al–Mn alloys containing less than 7 at % Mn

YIBIN ZHANG, TOSHIMI YAMANE, SHIGEOKI SAJI
Department of Materials Science and Engineering, Faculty of Engineering, Osaka University, 2-1 Yamadaoka, Suita Osaka 565, Japan

JUNZO TAKAHASHI
Department of Dental Technology, Faculty of Dentistry, Osaka University, 1-8 Yamadaoka, Suita Osaka 565, Japan

Morphology and enthalpy differences between a non-equilibrium state of as-melt spun ribbons and the equilibrium state of fully annealed ribbons were investigated by TEM observation, X-ray analysis and differential scanning calorimetry (DSC) measurements for Al–1.66, 2.56, 3.95, 5.37 and 6.98 at % Mn alloys. The icosahedral phase was observed with α–Al solid solution in as-melt spun 3.95, 5.37 and 6.98 at % Mn ribbons. The morphology of the icosahedral phase was complex; small particles, petal-like or coral-like branches and eutectic structure within the cell and small particles, films and networks along cell boundaries were observed depending on the manganese content. The differential enthalpy, $d(\Delta H_0^{ne})/dT$, versus T curve obtained by characteristic DSC measurements normally showed three peaks. The peak P_1 at 520–560 K corresponds to the precipitation and growth of the icosahedral phase, the peak P_2 at about 600–800 K to the transformation from the icosahedral phase to the equilibrium Al_6Mn phase, and the peak P_3 at about 700–880 K to the precipitation of Al_6Mn from α-Al solid solution. The temperatures of the peaks P_2 and P_3 shift to the lower side and the height of the peaks becomes higher with increasing manganese content. The enthalpy difference due to the fine microstructure in as-melt spun ribbons was also estimated.

1. Introduction

Since the icosahedral phase with fivefold symmetry was detected in rapidly solidified Al–14 at % Mn alloy by Shechtman *et al.* [1], a number of studies on rapidly solidified Al–Mn alloys have been reported [2–7]. The icosahedral phase is a non-equilibrium and quasi-crystalline phase which is quasi-periodic in three dimensions. There is another type of quasi-crystalline phase referred to as the decagonal or T-phase [2], which is quasi-periodic in two dimensions. The icosahedral phase was formed during rapid solidification by the nucleation and growth mechanism in Al–(6–22.5) at % Mn alloys [3–8]. The decagonal or T-phase was also formed in as-melt spun Al–(17–22.5) at % Mn ribbons [4]. The morphology of rapidly solidified Al–Mn alloys is very complex [9–11] and it may depend on the manganese content, local cooling rates and solute segregation. There is no report on the formation of the icosahedral and decagonal phases in rapidly solidified Al–Mn alloys containing manganese less than 6 at %. Details of the microstructures in as-melt spun ribbons of Al–Mn alloys with low manganese content are not clear.

The enthalpy of a rapidly solidified alloy in a non-equilibrium state is different from that of a fully annealed alloy in the equilibrium state, and the enthalpy difference exists between the two states at room temperature, mainly dependent on the degree of decomposition during rapid solidification. It is very difficult to evaluate this enthalpy difference by determining the latent heats for various phase transformations at the instant of rapid solidification.

In the present work, details of the microstructures formed during melt-spinning of various Al–Mn alloys containing (1.66–6.98) at % Mn were investigated, and a method of evaluating the enthalpy difference between as-melt spun ribbons and fully annealed ribbons using a technique based on differential scanning calorimetry (DSC) measurements was proposed.

2. Experimental procedure

2.1. Sample preparation

Al–1.66, 2.56, 3.95, 5.37 and 6.98 at % Mn alloys were prepared in alumina crucibles from pure aluminium (99.993 wt %) and manganese (99.99 wt %). These molten alloys, at temperatures higher than 1100 K, were squirted with argon gas of 80 kPa in pressure on to a copper wheel with a diameter of 153 mm. The wheel was rotated at a surface velocity of 17 m s^{-1} for

0022–2461

Al–1.66 and 2.56 at % Mn alloys, and 36 m s^{-1} for Al–3.95, 5.37 and 6.98 at % Mn alloys. The continuous ribbons obtained had a sectional shape of 3–4 mm in width and 45–80 μm in thickness. In this case the cooling rate may be in the range from 10^5 to 10^6 K s^{-1}, because a cooling rate of (0.5–2) $\times 10^5$ K s^{-1} has been calculated using the secondary dendrite arm spacing and a temperature gradient of 10^2–10^4 K mm^{-1} for Al–Cu alloy ribbons with a thickness of 80–120 μm in this single roller method [11]. As-melt spun ribbons were sealed in a silica tube under vacuum for annealing.

2.2. TEM observation and X-ray analysis

Microstructural observation was performed in a transmission electron microscope (JEM 2000EX) operated at 125 kV for specimens thinned by twin-jet electropolishing in a methanol solution containing 8 wt % $HClO_4$ and 37 vol % glycerine. X-ray analysis was carried out by an X-ray diffractometer (Rigaku D3F) using graphite-monochromatized CuK_α radiation at 33 kV and 22 mA to identify phases.

2.3. Estimation of enthalpy differences

The enthalpy differences at room temperature between a non-equilibrium state of rapidly solidified Al–Mn ribbons and the equilibrium state of fully annealed ribbons is estimated based on the data of DSC measurements. DSC measurements were carried out at a heating rate of 0.2 K s^{-1} from 310 to 860 K in a Rigaku PTC-10 apparatus. The instrumental constant was estimated by measuring the heat of fusion and the melting point of pure tin, zinc and lead. (37–40 mg) of as-melt spun ribbon and 40 mg of pure aluminium (99.993 wt %) (reference material) were individually packed in aluminium pans for DSC measurements.

In order to evaluate the enthalpy difference, ΔH_0^{ne}, we consider two thermodynamic processes illustrated in Fig. 1. *Process 1* involves continuous heating of fully annealed alloys in the equilibrium state from room temperature, T_0, to a temperature T_1, and then from the T_1 to the melting point T_m; the enthalpy changes corresponding to the above-mentioned temperature range are ΔH_1 and ΔH_2 in this reversible process. *Process 2* involves continuous heating of an as-rapidly solidified alloy in a non-equilibrium state from room temperature, T_0, to temperature T_1 and then from the T_1 to the melting point T_m, the corresponding enthalpy changes being ΔH_1^{ne} and ΔH_2^{ne} in this irreversible process, respectively. ΔH_0^{ne} is given by the equation

$$-\Delta H_0^{ne} + \Delta H_1^{ne} + \Delta H_2^{ne} = \Delta H_1 + \Delta H_2 \quad (1)$$

Assuming that $\Delta H_2^{ne} = \Delta H_2$ when the temperature T_1 approaches sufficiently close to the melting point T_m, Equation 2 below should follow from Equation 1:

$$\Delta H_0^{ne} = \Delta H_1^{ne} - \Delta H_1 \quad (2)$$

Thus, ΔH_0^{ne} can be evaluated from the difference of the two enthalpy changes, ΔH_1^{ne} and ΔH_1.

Two DSC runs were performed to carry out the thermodynamic calculation of Equation 2. In the first DSC run the DSC signal, $D^{ne}(T)$, of an as-melt spun ribbon was measured up to 860 K (T_1). After Mraw [12], $D^{ne}(T)$ is the differential heat flow between the sample and reference in the DSC apparatus, and it can be expressed by the equation

$$\kappa D^{ne}(T) = \frac{dQ_s^{ne}}{d\tau} - \frac{dQ_r}{d\tau} \quad (J\,s^{-1}) \quad (3)$$

where κ is the instrumental constant of the DSC

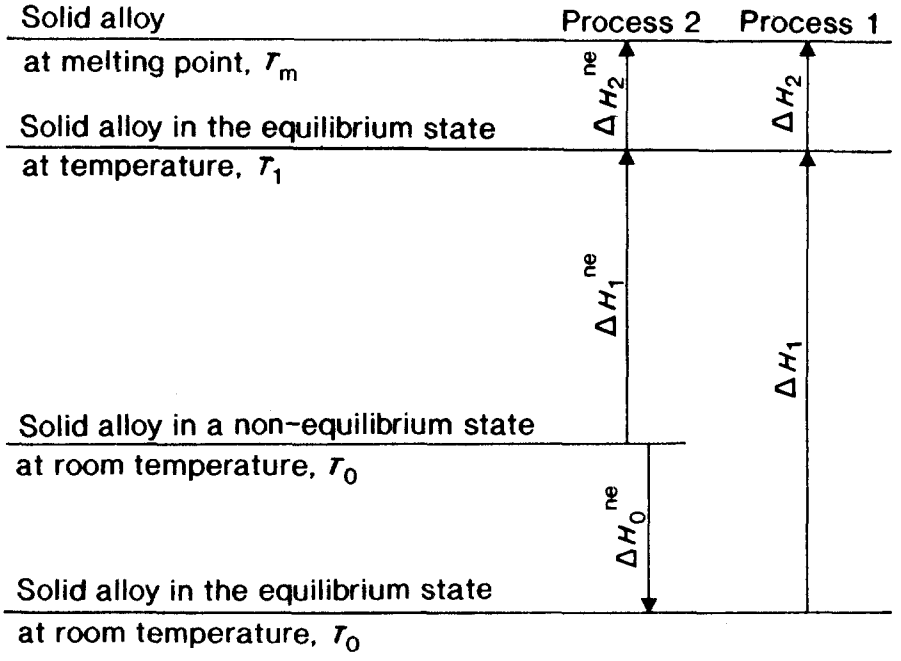

Figure 1 Schematic illustration of enthalpy changes during continuous heating of solid alloy in the equilibrium state, (process 1) and in a non-equilibrium state (process 2).

apparatus used, $dQ_s^{ne}/d\tau$ is the heat flow from the heater to the sample, and $dQ_r/d\tau$ is the heat flow from the heater to the reference.

After the first run the sample was held at 890 K for 1.2 ks, cooled to 760 K at a cooling rate of 3.6×10^{-2} K s^{-1}, held at 760 K for 7.2 ks, and then slowly (1.3×10^{-2} K s^{-1}) cooled to room temperature. The sample after the above-mentioned heat treatments should be in the fully annealed and equilibrium state. The DSC signal, $D^e(T)$, for the second run can be written as

$$\kappa D^e(T) = \frac{dQ_s^e}{d\tau} - \frac{dQ_r}{d\tau} \quad (J\ s^{-1}) \tag{4}$$

The following thermodynamic relationship:

$$\left(\frac{\partial H}{\partial T}\right)_p = \left(\frac{dQ}{dT}\right)_p \tag{5}$$

is advisable for the isobaric process; thus, we can write

$$\frac{dQ_s^{ne}}{d\tau} = \frac{dT}{d\tau}\left(\frac{dQ_s^{ne}}{dT}\right) = \frac{dT}{d\tau}\left(\frac{d(\Delta H_1^{ne})}{dT}\right) \tag{6}$$

$$\frac{dQ_s^e}{d\tau} = \frac{dT}{d\tau}\left(\frac{dQ_s^e}{dT}\right) = \frac{dT}{d\tau}\left(\frac{d(\Delta H_1)}{dT}\right) \tag{7}$$

Hence, Equation 8 can be obtained finally by combining Equations 2, 6 and 7:

$$\frac{d(\Delta H_0^{ne})}{dT} = \left(\frac{\kappa}{\beta}\right)[D^{ne}(T) - D^e(T)] \quad (J\ mol^{-1}\ K^{-1}) \tag{8}$$

where $\beta = dT/d\tau$ is the heating rate of DSC measurements and $\kappa = 0.8$ for $\beta = 0.2$ K s^{-1} in this work. We can calculate the value of $(\kappa/\beta)[D^{ne}(T) - D^e(T)]$ from data of the two DSC curves and plot a $d(\Delta H_0^{ne})/dT$ versus T curve. The definite integral of $d(\Delta H_0^{ne})/dT$ is expressed by Equation 9 below, and ΔH_0^{ne} gives the enthalpy difference between non-equilibrium state of as-melt spun ribbon and the equilibrium state of fully annealed ribbon at room temperature:

$$\Delta H_0^{ne} = \int_{T_0}^{T_1}\left(\frac{\kappa}{\beta}\right)[D^{ne}(T) - D^e(T)]\,dT \quad (J\ mol^{-1}\ K^{-1}) \tag{9}$$

3. Results and discussion

3.1. Microstructural morphology of the icosahedral phase

The icosahedral phase was confirmed in as-melt spun ribbons of Al–3.95, 5.37 and 6.98 at % Mn alloys by means of TEM, and it was not observed in Al–1.66 and 2.56 at % Mn ribbons. By X-ray diffraction measurements, the icosahedral phase was not detected in as-melt spun ribbons of Al–Mn alloys containing up to 5.37 at % Mn, and weak peaks of the icosahedral phase were detected together with peaks corresponding to the supersaturated α-Al solid solution in Al–6.98 at % Mn ribbons. The 6.98 at % Mn ribbons showed α-Al (2 2 2) peaks which were split, indicating two different concentrations of solid solution. These ribbons seem to contain some regions of supersaturated solid solution and other regions which contain icosahedral phase plus manganese-depleted aluminium, as described by Schaefer *et al.* [4] and Yu-Zhang *et al.* [8].

A morphological variety of the icosahedral phase was observed. The typical structures in 3.95 at % Mn ribbons are shown in Fig. 2. Fig. 2a shows the icosahedral phase particles at cell boundaries and films (arrows) along cell boundaries. No particles were

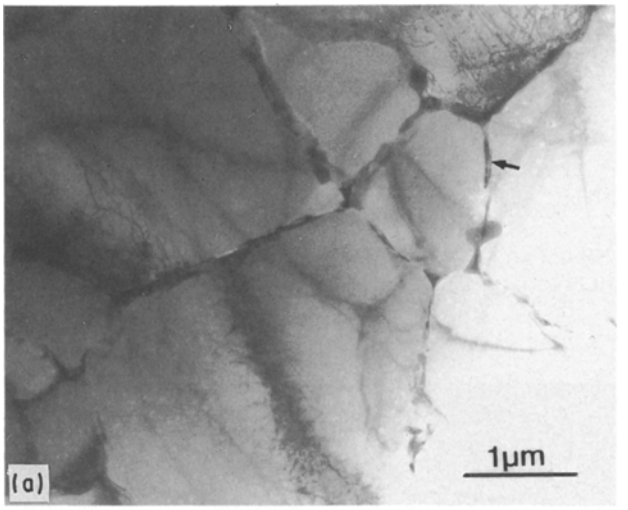

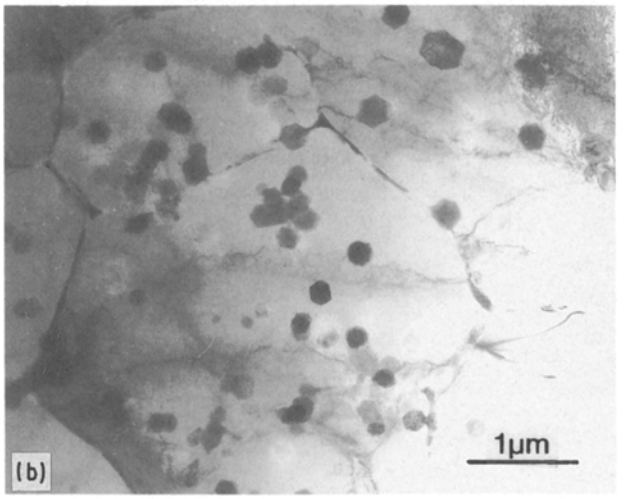

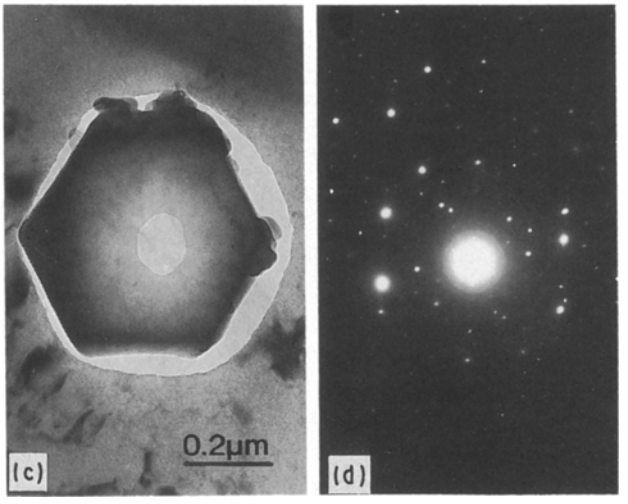

Figure 2 TEM micrographs of the icosahedral phase in as-melt spun Al–3.95 at % Mn ribbon: (a) the icosahedral phase at the cell boundaries, (b) small particles of the icosahedral phase within the cells, (c) enlarged photograph of an icosahedral phase particle, (d) SADP from the particles in (b).

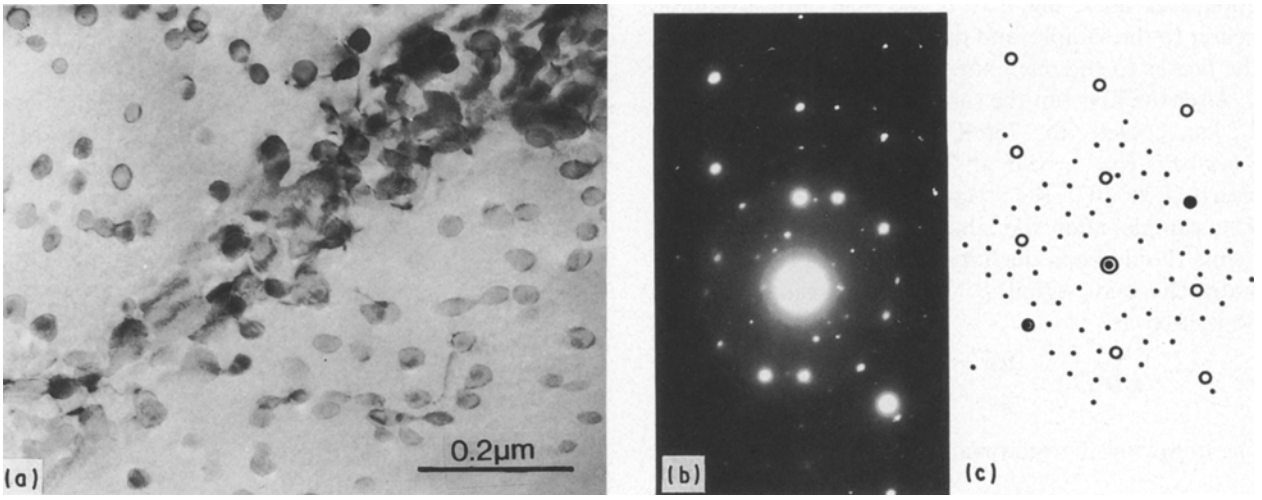

Figure 3 (a) TEM micrograph of icosahedral phase particles in as-melt spun Al–5.37 at % Mn ribbon, (b) SADP from the particles with α-Al [0 $\bar{2}$ 2] zone axis, (c) schematic diagram of SADP showing the icosahedral phase; (○) α-Al [0 $\bar{2}$ 2].

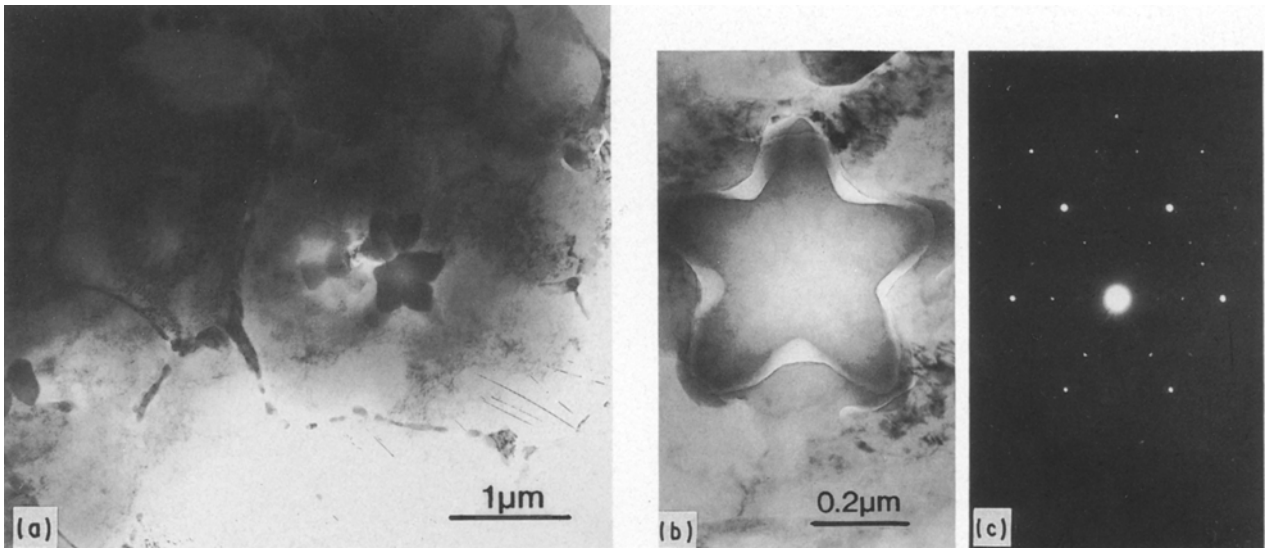

Figure 4 (a, b) TEM micrographs of petal-like branches and (c) SADP, in as-melt spun Al–5.37 at % Mn ribbon.

observed within the grains in some regions where the local cooling rate may have been large. On the other hand, there are many particles of the icosahedral phase in the grains shown in Fig. 2b. These particles of the icosahedral phase appear as small hexagonal rods in external shape as seen in Fig. 2b and c. Fig. 2d is a selected-area diffraction pattern (SADP) from the particles, showing the icosahedral phase.

In as-melt spun Al–5.37 at % Mn ribbons, small spherical particles, petal-like branches and networks at cell boundaries of the icosahedral phase were observed. Fig. 3a shows spherical particles (about 30 to 50 nm in diameter) of the icosahedral phase as confirmed by the SADP in Fig. 3b and c; these particles have the same orientation relationships. Fig. 4a shows petal-like branches within cells and the icosahedral phase at or along cell boundaries. A larger view of the petal-like branches and its SADP are shown in Fig. 4b and c, respectively. Networks of the icosahedral phase formed along cell boundaries during rapid solidification are shown in Fig. 5a. Fig. 5b indicates that the networks of icosahedral phase grow larger after annealing at 490 K for 14.4 ks, and the amount of the networks was observed to increase remarkably after the annealing.

In Al–6.98 at % Mn ribbons, the morphology of the icosahedral phase showed coral-like branches, fine eutectic structure and small particles with a supersaturated α-Al matrix. Fig. 6a shows the coral-like branches (marked A) surrounded by α-Al solid solution (B) and fine eutectic structure (C) (refer also to Fig. 6b). The coral-like branches appear as the primary crystal, and the fine eutectic structure is formed by non-equilibrium eutectic reaction in terms of coupled growth [11] between the supersaturated α-Al solid solution and the icosahedral phase. Fig. 6c is an SADP obtained from the coral branches in Fig. 6a, showing the icosahedral phase with fivefold symmetry. Fig. 6d is an SADP from the fine eutectic structure in Fig. 6b, also showing the icosahedral phase.

A chain reaction of the small icosahedral particles occurred at the dendritic cell boundaries of supersaturated α-Al solid solution in rapidly solidified Al–6.98 at % Mn ribbon, as shown in Fig. 7. The

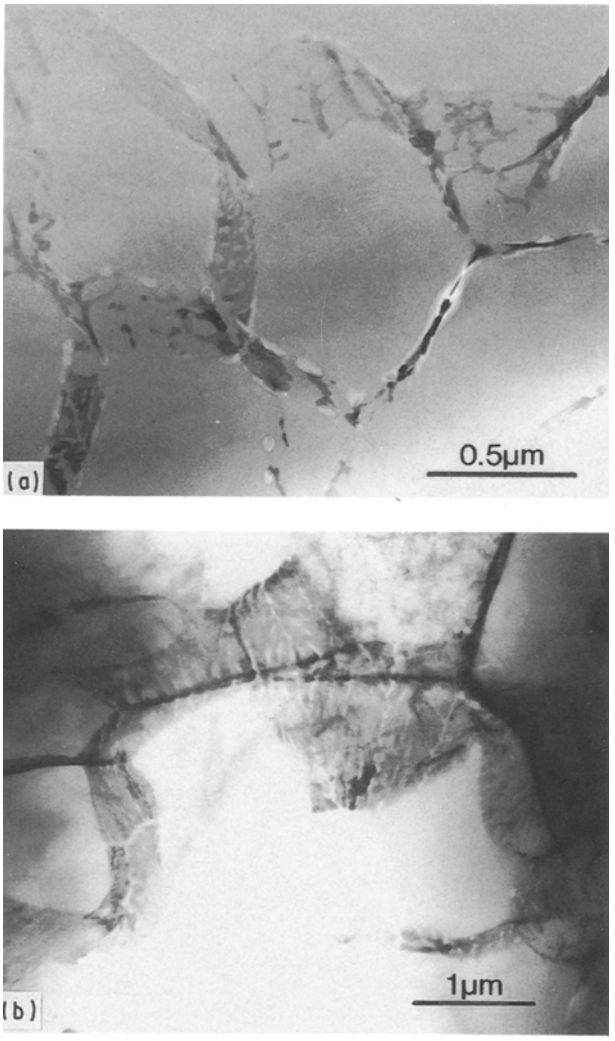

Figure 5 TEM micrographs of networks of icosahedral phase along cell boundaries in Al–5.37 at % Mn alloy: (a) as-melt spun ribbon, (b) ribbon annealed at 490 K for 14.4 ks, showing the growth of the networks during annealing.

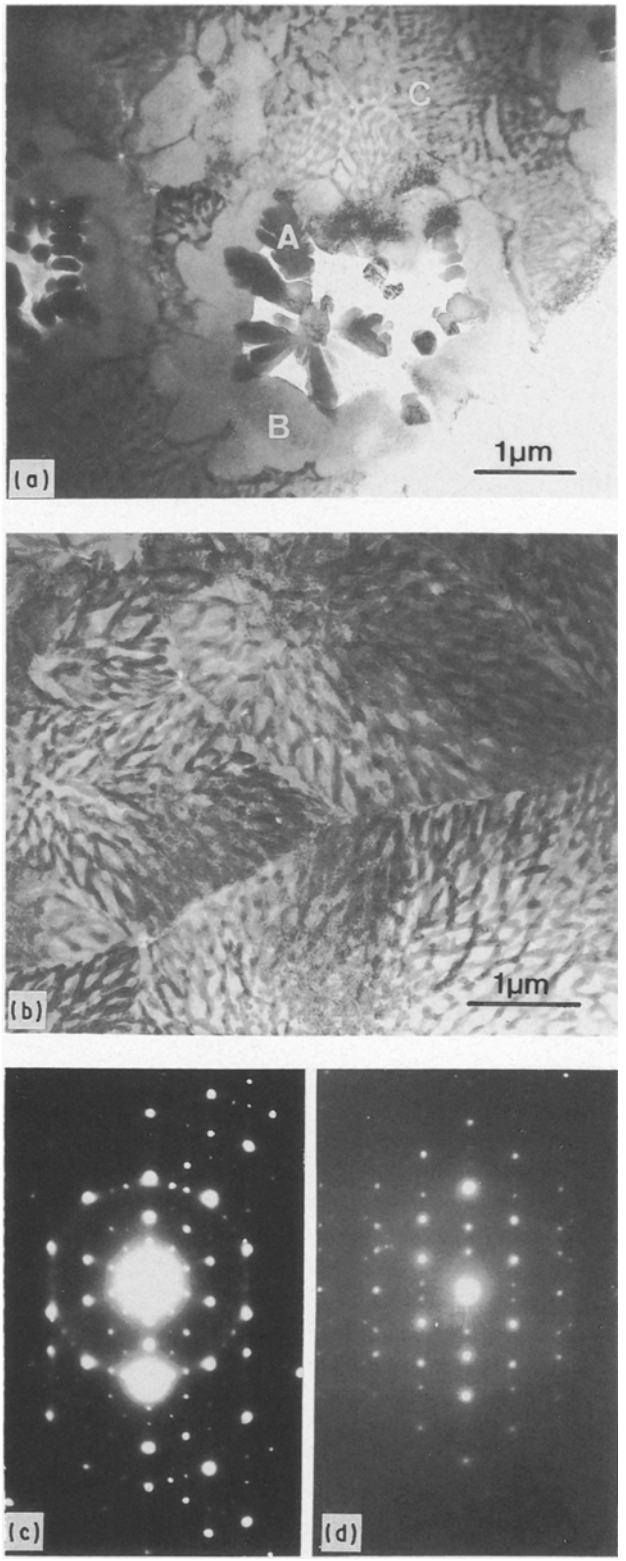

Figure 6 TEM micrographs and SADP in as-melt spun Al–6.98 at % Mn ribbon: (a) showing petal-like branches (marked A) surrounded by supersaturated α-Al solid solution (marked B) and eutectic structure (marked C) in as-melt spun Al–6.98 at % Mn ribbon; (b) enlarged photograph of the eutectic structure; (c) SADP from the petal-like branch in (a) showing the icosahedral phase; (d) SADP from the eutectic structure in (b) showing the icosahedral phase.

linkage of the icosahedral phase particles which were left after elution of the α-Al solid solution by a corrosive solution are vividly observed in Fig. 7b and d. Fig. 7e is an SADP from Fig. 7b showing that the small particles formed at the cell boundaries are the icosahedral phase.

It has been pointed out by Shechtman and Blech [3] that the icosahedral phase has a composition close to Al_6Mn. Therefore, a large change in manganese composition in the melt seems to be necessary to form the icosahedral phase by the nucleation and growth mechanism during rapid solidification of Al–3.95, 5.37 and 6.98 at % Mn ribbons. When the icosahedral phase first solidifies in a manganese rich region of the melt, the petal-like or coral-like branches would be formed and then the α-Al solid solution might solidify surrounding them. When dendritic cells of the supersaturated α-Al solid solution are formed as primary crystals, large concentration gradients exist in the tip region of the cellular array [13] and a large segregation of manganese atoms occurs at the valleys of cellular arrays.

Thus linkages or networks of the icosahedral phase might be formed as a second solidified phase under an appropriate local cooling rate at cellular valleys, as shown by a schematic illustration in Fig. 8. The segregation of manganese in the tip regions of cellular arrays also results in an inhomogeneous distribution

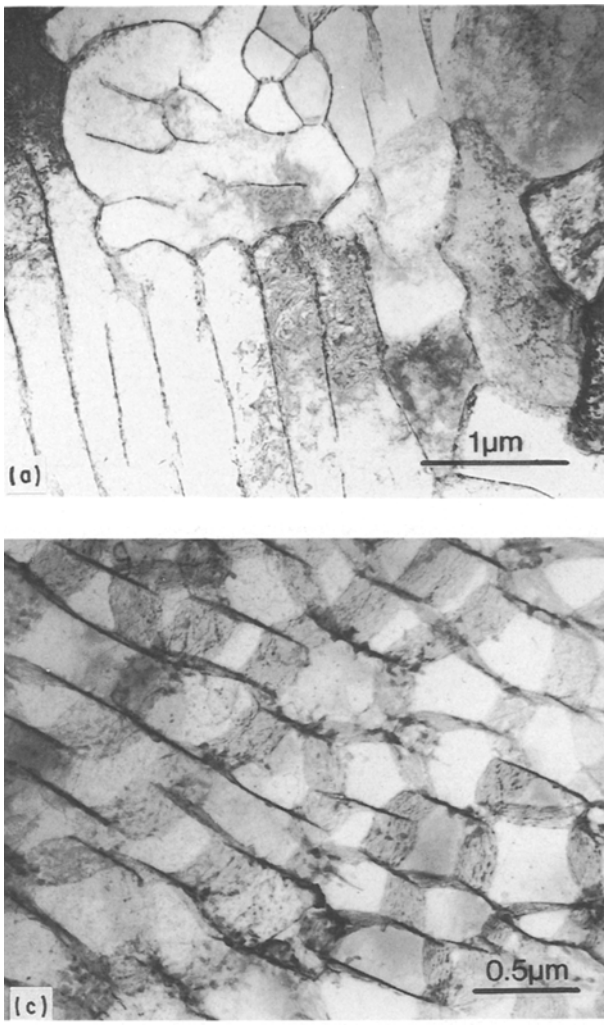

Figure 7 (a, c) TEM micrographs of dendritic cells of α-Al solid solution; (b, d) linkage of icosahedral phase particles along the boundaries obtained after elution of the α-Al solid solution; (e) SADP from (b) showing the icosahedral phase for as-melt spun Al–6.98 at % Mn ribbon.

of manganese in the transverse section of supersaturated α-Al solid solution cells, i.e. the manganese concentration in the vicinity of cell boundaries is higher than that in the centre of cells; thus, precipitation of the icosahedral phase and growth of the icosahedral phase networks preferentially occur in the vicinity of cell boundaries or along cell boundaries. The fine eutectic structure formed by a non-equilibrium eutectic reaction between supersaturated α-Al solid solution and the icosahedral phase is similar to the non-equilibrium eutectic structures in as-melt spun Al–Cu [11, 14], Al–Fe [15], Al–Fe–Ni [16] and Mg–Si [17] alloys with non-eutectic compositions.

3.2. Calorimetric evaluation of non-equilibrium state

The $d(\Delta H_0^{ne})/dT$–T curves obtained by the characteristic DSC measurements described in detail in Section 2 are illustrated in Fig. 9 for rapidly solidified Al–1.66, 2.56, 3.95, 5.37 and 6.98 at % Mn alloys. The curves show the releases of enthalpy with continuous heating temperature. There is one broad peak corresponding to precipitation of the equilibrium Al_6Mn phase from the supersaturated α-Al solid solution at about 820 K for 1.66 at % Mn alloy [8, 9]. On the other hand, three peaks, P_1, P_2 and P_3, can be seen on each of the curves for 3.95, 5.37 and 6.98 at % Mn alloys. The peak P_1 appears at temperatures from about 540 to 560 K, and the peak height is the lowest of the three peaks for each alloy. The peaks P_2 and P_3 become higher and both peak temperatures shift to the lower

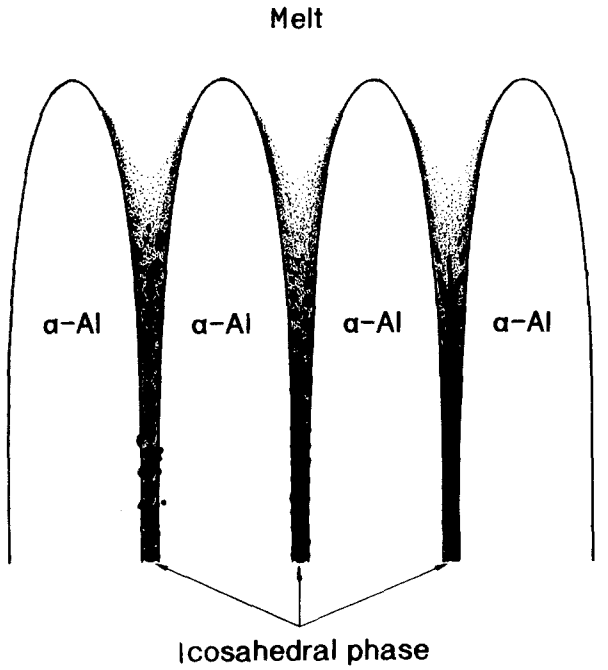

Figure 8 Schematic illustration of the formation of networks or linkages of icosahedral phase at dendritic cell boundaries of α-Al solid solution which is attributed to large segregation of manganese atoms in the liquid phase in the vicinity of solidification fronts.

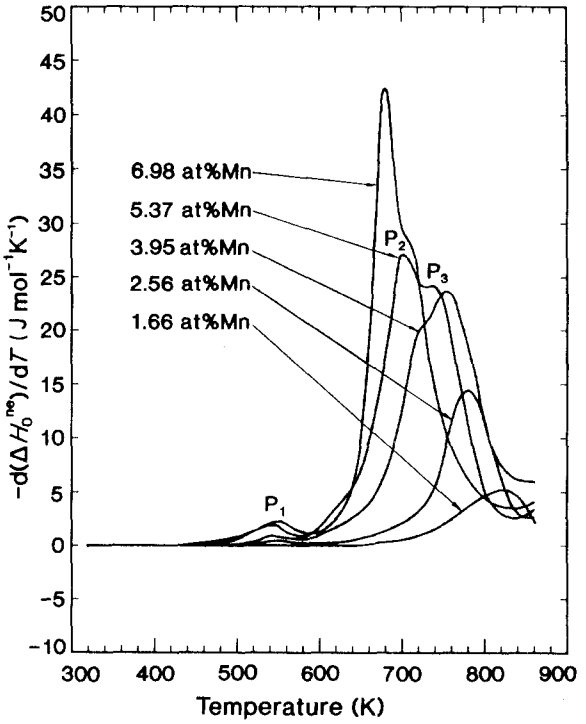

Figure 9 $d(\Delta H_0^{ne})/dT$–T curves obtained by characteristic DSC measurements during continuous heating at 0.2 K s^{-1} for Al–1.66, 2.56, 3.95, 5.37 and 6.98 at % Mn alloys.

side with increasing manganese content. The peaks on the $d(\Delta H_0^{ne})/dT$–T curves imply intensive releases of enthalpy on phase transformations in melt-spun ribbons in a non-equilibrium state.

According to other reports on phase transformations during continuous heating of melt-spun ribbons of Al–Mn alloys by DSC measurements [8, 9, 18], the peak occurring at about 550 K on DSC curves corresponds to precipitation of the icosahedral phase in the supersaturated α-Al solid solution. In the present work, the peak P_1 at about 500–580 K may be due to the precipitation and growth of networks of icosahedral phase at cell boundaries. Growth of the networks is clearly observed after annealing at 490 K for 14.4 ks, as shown in Fig. 5b. The peaks P_2 and P_3 in the temperature range from 600 to 820 K (depending on manganese content) are attributed to transformation of the icosahedral phase to the equilibrium Al_6Mn phase and precipitation of the Al_6Mn and G phases from the supersaturated α-Al solid solution, respectively [8, 9, 18]. The peaks P_2 and P_3 shift to higher temperatures and the peak heights are reduced with increasing manganese content.

The values of the enthalpy difference between a non-equilibrium state of as-rapidly solidified ribbon and the equilibrium state of the fully annealed ribbon at room temperature, ΔH_0^{ne}, are plotted against manganese content for the alloys used in Fig. 10. ΔH_0^{ne} increases with increasing manganese content, and the trend of ΔH_0^{ne} increment is remarkable in the range from about 2 to 4 at % Mn. The value of ΔH_0^{ne} is in the range from -2.8 to -3.5 kJ mol^{-1} for Al–(3.95–6.98) at % Mn alloys. These values are not negligible compared with the latent heat for solidification, 10.47 kJ mol^{-1} [19], of pure aluminium.

ΔH_0^{ne} is attributed to the incomplete release of solidification latent heats for various phase transformations during rapid solidification. This energy might be stored in a non-equilibrium state consisting of the supersaturated α-Al solid solution, metastable phases, interfaces of different phases, fine cell boundaries and so on, in as-rapidly solidified ribbons.

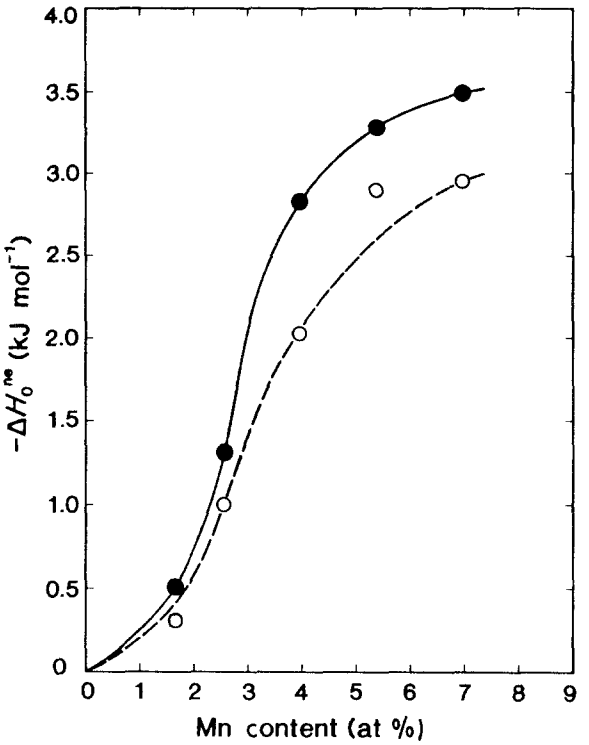

Figure 10 Changes in enthalpy differences with manganese conten.. (●) ΔH_0^{ne}, the total value of enthalpy difference; (○) $(\Delta H_0^{ne})'$, enthalpy difference calculated from the total area of the peaks on each curve in Fig. 9.

The broken line in Fig. 10 shows the change in the value of $(\Delta H_0^{ne})'$, obtained from the total area of the

three peaks, with manganese content, which corresponds to the energy stored in various kinds of non-equilibrium phase. Therefore, the difference between the solid and broken lines in Fig. 10 seems to be the energy stored in the fine microstructures. The difference is very small for Al–1.66 and 2.65 at % Mn alloys, and comparatively large and nearly the same for Al–3.95, 5.37 and 6.98 at % Mn alloys. The latter large value is due to the development of fine cell structure, eutectic structure and networks of the icosahedral phase at cell boundaries. The enthalpy difference, $\Delta H_0^{ne} - (\Delta H_0^{ne})'$, due to the fine microstructures is at its utmost about 30% of the total value of ΔH_0^{ne} for Al–3.95 at % Mn alloy.

4. Conclusions

1. Only supersaturated α-Al solid solution was observed in as-melt spun Al–1.67 and 2.56 at % Mn ribbons, and the icosahedral phase was observed with supersaturated α-Al solid solution in as-melt spun Al–3.95, 5.37 and 6.98 at % Mn ribbons.

2 The morphology of the icosahedral phase shows petal-like or coral-like branches in grains of supersaturated α-Al solid solution, small particles within or at cell boundaries, films and networks along cell boundaries, and fine eutectic structure. The complex morphology of the icosahedral phase may be due to the segregation of manganese atoms and differences in local cooling rates.

3. The enthalpy difference at room temperature between a non-equilibrium state of as-melt spun ribbon and the equilibrium state of the fully annealed ribbon was evaluated using a special DSC measurement method. The enthalpy difference obtained increased with increasing manganese content in Al–Mn ribbons and the trend of the increment became remarkable in the range from about 2 to 4 at % Mn.

4. The energy stored in as-melt spun ribbons with fine microstructure (fine cells, eutectic structure and networks of the icosahedral phase) was also estimated. The result obtained showed good agreement with the dependence of the observed microstructures on the manganese content in Al–Mn alloys.

Acknowledgements

Yibin Zhang would like to thank the Japanese government (the Ministry of Education, Science and Culture) for a scholarship, and Mr Y. Sato for supporting the operation of the transmission electron microscope.

References

1. D. SHECHTMAN, I. BLECH, D. GRATIAS and J. W. CAHN, *Phys. Rev. Lett.* **53** (1984) 1951.
2. L. A. BENDERSKY, *ibid.* **55** (1985) 1461.
3. D. SHECHTMAN and I. A. BLECH, *Metall. Trans.* **16A** (1985) 1005.
4. R. J. SCHAEFER, L. A. BENDERSKY, D. SHECHTMAN, W. J. BOETTINGER and F. S. BIANCANIELLO, *ibid.* **17A** (1986) 2117.
5. J. A. JUAREZ-ISLAR, D. H. WARRINGTON and H. JONES, *J. Mater. Sci.* **24** (1989) 2076.
6. F. H. SAMUEL, A. M. SAMUEL, A. de JONCKERE and F. GERIN, *Metall. Trans.* **17A** (1986) 1671.
7. A. INOUE, L. ARNBERG, B. LEHTINEN, M. OGUCHI and T. MASUMOTO, *ibid.* **17A** (1986) 1657.
8. K. YU-ZHANG, M. HARMELIN, A. QUIVY, Y. CALVAYRAC, J. BIGOT and R. PORTIER, *Mater. Sci. Engng* **99** (1988) 385.
9. K. F. KOBAYASHI, H. KAWAURA and P. H. SHINGU, in "Aluminum Alloys–Physical and Mechanical Properties", Vol. 1, edited by E. A. Starke and T. H. Sanders (EMAS, Warley, 1986) p. 247.
10. S. R. NISHITANI, H. KAWAURA, K. F. KOBAYASHI and P. H. SHINGU, *J. Cryst. Growth* **76** (1986) 209.
11. Y. ZHANG, T. YAMANE, K. HIRAO and Y. MINAMINO, *J. Mater. Sci.* **26** (1991) 5799.
12. S. C. MRAW, *Rev. Sci. Instrum.* **53** (1982) 228.
13. B. GIOVANOLA and W. KURZ, *Z. Metall.* **82** (1991) 83.
14. B. A. MUELLER and J. H. PEREPEZKO, *Mater. Sci. Engng* **98** (1988) 153.
15. W. J. BOETTINGER, L. BENDERSKY and J. G. EARLY, *Metall. Trans.* **17A** (1986) 781.
16. W. J. BOETTINGER, L. A. BENDERSKY, R. J. SCHAEFER and F. S. BIANCANIELLO, *ibid.* **19A** (1988) 1101.
17. F. C. GRENSING and H. L. FRASER, *Mater. Sci. Engng* **98** (1988) 313.
18. M. HARMELIN and J. JIANG, *Thermochim. Acta* **162** (1990) 453.
19. E. A. BRANDES (ed.), "Smithells Metals Reference Book" 6th Edn (Butterworths, London, 1983) p. 8–1.

Received 3 March
and accepted 17 November 1992